JOURNAL OF GEOPHYSICAL RESEARCH, VOL. 111, B07202, doi:10.1029/2005JB004098, 2006

Discontinuous evolution of single-crystal elastic constants as a function of pressure through the $C2/c \leftrightarrow P2_1/c$ phase transition in spodumene ($LiAlSi_2O_6$)

Peter Sondergeld,[1] Baosheng Li,[2] Jürgen Schreuer,[3] and Michael A. Carpenter[1]

Received 10 October 2005; revised 9 February 2006; accepted 1 March 2006; published 12 July 2006.

[1] A Landau free energy expansion in one order parameter has been developed to describe the first-order $C2/c \leftrightarrow P2_1/c$ phase transition at high pressures in spodumene ($LiAlSi_2O_6$). The complete set of elastic constants required for this model was determined at ambient conditions by resonant ultrasound spectroscopy. Other coefficients in the 246 expansion were calibrated using lattice parameter data from the literature, which had been collected by following the transition in a diamond anvil cell. The complete calibration leads to predictions of significant, abrupt changes in elastic constants at the transition point, 3.19 GPa, which have then been tested against ultrasonic data obtained in situ at high pressures in a uniaxial split cylinder apparatus. Velocities of compressional waves in three mutually perpendicular directions through single crystals of spodumene were measured and used to extract elastic constant data. The transition, indeed, causes large, abrupt changes of single-crystal elastic constants with increasing pressure. Steep increases in attenuation were also observed in the vicinity of the transition point for two directions and over a broader pressure interval in the third direction. The Landau expansion reproduces the general form of the elastic anomalies, even though it does not do as well for spontaneous strain variations. If this type of transition occurred in mantle pyroxenes (or in any other mantle phase), it would be expected to leave a distinctive signature in seismic velocity profiles of the Earth's interior.

Citation: Sondergeld, P., B. Li, J. Schreuer, and M. A. Carpenter (2006), Discontinuous evolution of single-crystal elastic constants as a function of pressure through the $C2/c \leftrightarrow P2_1/c$ phase transition in spodumene ($LiAlSi_2O_6$), *J. Geophys. Res.*, *111*, B07202, doi:10.1029/2005JB004098.

1. Introduction

[2] Over substantial depth intervals through the mantle the elastic properties of minerals evolve smoothly under the normal influence of thermal expansion and compressibility. Discontinuities or other anomalies between zones with smooth variations have generally been understood as being due to changes in composition and/or mineral assemblage. The magnitude of a given anomaly and the depth range over which it occurs will depend on differences in the elastic constants of minerals across a reconstructive transformation, such as olivine ↔ wadsleyite, and the *PT* interval over which the divariant assemblage of reactant plus product phases remains stable [e.g., *Agee*, 1998, and references therein]. Another quite different class of anomaly might also occur, however, in which composition and mineral assemblage remain the same but an individual mineral undergoes a displacive phase transition. It is well known from extensive studies of a wide range of materials that displacive transitions can be accompanied by changes in elastic constants on the order of tens of percent [e.g., *Carpenter and Salje*, 1998, and references therein]. This is the case even when changes in other properties, such as lattice dimensions and density, are below 1%. Given that many rock forming silicates are susceptible to structural instabilities of this type, it would be rather surprising if every mineral in the mantle remained in the stability field of only one of its polymorphs for the entire *PT* range over which it is present. The question then arises as to how seismic anomalies due to displacive transitions might be recognized. In a previous paper [*Carpenter et al.*, 2000], Landau theory was used to show how a proper ferroelastic transition in stishovite would contribute to elastic softening over a wide pressure interval. The purpose of the present paper is to show how a coelastic transition could give rise to substantial discontinuities in bulk elastic properties.

[3] The pyroxene spodumene, $LiAlSi_2O_6$, is hardly likely to be a mantle phase. On the other hand, it undergoes a $C2/c \rightarrow P2_1/c$ transition at a pressure (~3.2 GPa) which is rather convenient for experimental investigation [*Arlt and Angel*, 2000a; *Pommier et al.*, 2003]. The same, or closely related transitions occur with increasing pressure in a

[1]Department of Earth Sciences, University of Cambridge, Cambridge, UK.
[2]Department of Geosciences, State University of New York at Stony Brook, Stony Brook, New York, USA.
[3]Institut für Mineralogie/Kristallographie, Universität Frankfurt, Frankfurt am Main, Germany.

0148-0227/06/2005JB004098$09.00

Table 1. Details of High Pressure Runs[a]

Run	Experiment	Direction of Compressional Waves	Oil Pressure: Bi_I, P_{tr} (spodumene), Bi_{II}, bars	P_{tr}, GPa	Buffer Rod Length, mm	Sample Length, mm
1	66	A	85, 150, 345	4.2	3.200(1)	2.038(1)
2	71	A	110, 145, 345	3.35	3.207(1)	2.031(1)
3	65	B	120, 170, 435	3.17	3.205(1)	1.658(1)
4	70	B	115, 155, 340(?)	3.6(?)	3.203(1)	1.819(1)
5	May 2002	C	112, 130, 390	2.975	2.93[b]	1.730(1)[b]
6	67	C	117, 135, 355	2.9	3.200(1)	2.007(1)

[a]Question marks indicate that the signal marking one of the transitions in Bi was not clear.
[b]Lengths were measured on recovered sample, after high-pressure experiment.

number of pyroxenes [*Arlt et al.*, 1998, 2000; *Arlt and Angel*, 2000a, 2000b]. More importantly in the present context, the transition in spodumene is representative of transitions in which there is no change in point group and in which the order parameter is associated with a special point on the Brillouin zone boundary. It is also first order in character and is thus expected to show a more marked elastic discontinuity at the transition point than would occur at a classical second-order transition. According to Landau theory it should show some elastic softening as the transition point is approached from within the stability field of the low symmetry phase, giving rise to a distinctive pattern of elasticity changes. Thanks to the diamond anvil cell diffraction measurements of *Arlt and Angel* [2000a], high-quality lattice parameter data are available for both the $C2/c$ and $P2_1/c$ structures. These have been used in the present study to calibrate a Landau free energy expansion for the transition. Essential for this calibration is a full set of elastic constants for the $C2/c$ structure and these have therefore been determined for a natural spodumene crystal at ambient conditions by resonant ultrasound spectroscopy (RUS). The Landau model is tested against experimental data collected in situ at pressures up to ~10 GPa for compressional and quasi-compressional acoustic velocities traveling parallel to three mutually perpendicular directions of single crystals.

2. Experimental Methods

2.1. Reference System

[4] Reference axes used here for formal descriptions of the elastic constants were chosen in order to be compatible with the spontaneous strain measurements of *Arlt and Angel* [2000a]. These, in turn, were derived from the original settings of the general strain equations of *Schlenker et al.* [1978]: **Y** parallel to the crystallographic *y axis*, **Z** parallel to the normal to the (001) plane (i.e., parallel to **c***), and **X** perpendicular to both [see also *Redfern and Salje*, 1987; *Carpenter et al.*, 1998a]. This differs from the reference system normally used to describe the elastic constants of a monoclinic crystal, which has **Y** parallel to the crystallographic *y axis*, **Z** parallel to the crystallographic *z axis* and **X** perpendicular to the (100) plane (i.e., parallel to **a***).

2.2. Sample Preparation

[5] All samples used for the high-pressure ultrasonic experiments were taken from a single, optically clear crystal of spodumene. The geological locality from which the crystal originally came is not known. Electron microprobe analysis gave Al and Si as the major elements with minor amounts of Na, Fe and Mn (Li is too light to be detected). Recalculating to 2 Si, and assuming 1 Li with Fe as Fe^{3+}, gave a chemical formula of $Li_{1.00}Na_{0.01}Mn_{0.002}Fe^{3+}_{0.005}Al_{0.97}Si_{2.00}O_6$. Well-developed crystal faces were used to help orient the crystal when sawing off three 2 mm thick slices in three mutually perpendicular directions. One slice was cut perpendicular to (010), at an angle of 40° from **c***. The second was cut perpendicular to [010]. The third was cut perpendicular to (010), at an angle of 40° from [100]. Cylinders, ~2.0 or ~2.25 mm in diameter, were cored from these slices and doubly polished by hand to 1 μm. The crystallographic orientation and final length of each polished cylinder used in six experimental runs are listed in Table 1. Length was measured to ±1 μm using a hand-held micrometer. An alumina buffer rod was also prepared for each high-pressure run in the form of a cylinder, 2.0 or 2.25 mm in diameter and 3.2 ± 0.01 mm long (except for run 5, 2.93 mm).

[6] Externally generated compressional waves in directions normal to the three slices, referred to below as directions A (40° from [100] in the (010) plane), B (parallel to [010]) and C (40° from **c*** in the (010) plane), have velocities determined by elastic constants C_A, C_B and C_C. These are related to formal elastic constants of the reference system used in this study according to (from the Christoffel equations)

$$C_A = \frac{1}{2}\left(\begin{array}{l} (C_{33}+C_{55})\cos^2(90-\alpha) + 2(C_{15}+C_{35})\cos(90-\alpha)\cos\alpha + (C_{11}+C_{55})\cos^2\alpha \\ + \sqrt{\begin{array}{l}\left((C_{33}+C_{55})\cos^2(90-\alpha) + 2(C_{15}+C_{35})\cos(90-\alpha)\cos\alpha + (C_{11}+C_{55})\cos^2\alpha\right)^2 \\ +4\left(\begin{array}{l}\left(C_{35}^2 - C_{33}C_{55}\right)\cos^4(90-\alpha) - 2(C_{15}C_{33}-C_{13}C_{35})\cos^3(90-\alpha)\cos\alpha \\ +\left(C_{13}^2 - C_{11}C_{33} - 2C_{15}C_{35} + 2C_{13}C_{55}\right)\cos^2(90-\alpha)\cos^2\alpha \\ +2(C_{13}C_{15}-C_{11}C_{35})\cos(90-\alpha)\cos^3\alpha + \left(C_{15}^2 - C_{11}C_{55}\right)\cos^4\alpha\end{array}\right)\end{array}}\end{array}\right) \quad (1)$$

$$C_B = C_{22} \quad (2)$$

Table 2. Density, Elastic Constants C_{ij}, Bulk Modulus K, Mean Elastic Stiffness C, and Elastic S Value of Monoclinic Spodumene and Diopside

	This Work		*Aleksandrov and Prodaivoda* [1993]	*Levien et al.* [1979]
	Standard Setting	Alternative Setting		
Compound	spodumene	spodumene	spodumene	diopside
Setting X, Y, Z	**a***, [010], [001]	[100], [010], **c***	unknown	**a***, [010], [001]
Density, g cm^{-3}	3.182	3.182	3.107	3.286[a]
C_{11}, GPa	280.5(3)	232.8	244.6	223
C_{22}	230.7(2)	230.7	198.9	171
C_{33}	303.0(4)	290.2	287.1	235
C_{44}	97.83(14)	103.3	70.1	74
C_{55}	68.76(8)	99.0	62.8	67
C_{66}	87.05(12)	81.6	70.7	66
C_{12}	94.3(2)	93.1	88.2	77
C_{13}	64.6(6)	94.8	63.9	81
C_{23}	91.6(3)	92.8	69.4	57
C_{15}	27.1(2)	32.2	−39.9	17
C_{25}	1.4(3)	1.9	−26.7	7
C_{35}	4.0(5)	−15.8	−14.2	43
C_{46}	10.4(2)	4.4	−7.1	7.3
K_{Reuss} [GPa]	143.9	143.9	116.8	108
K_{Voigt}	146.1	146.1		
C [GPa]	146.5	146.5	128.4	117
S [10^{-20} Nm]	1423	1423	1277	1284

[a]Calculated from lattice constants and chemical composition.

$$C_C = \frac{1}{2}\left((C_{33}+C_{55})\cos^2\alpha + 2(C_{15}+C_{35})\cos(90+\alpha)\cos\alpha + (C_{11}+C_{55})\cos^2(90+\alpha) + \sqrt{\left((C_{33}+C_{55})\cos^2\alpha + 2(C_{15}+C_{35})\cos(90+\alpha)\cos\alpha + (C_{11}+C_{55})\cos^2(90+\alpha)\right)^2 + 4\left(\left(C_{35}^2 - C_{33}C_{55}\right)\cos^4\alpha - 2(C_{15}C_{33} - C_{13}C_{35})\cos(90+\alpha)\cos^3\alpha + \left(C_{13}^2 - C_{11}C_{33} - 2C_{15}C_{35} + 2C_{13}C_{55}\right)\cos^2(90+\alpha)\cos^2\alpha + 2(C_{13}C_{15} - C_{11}C_{35})\cos\alpha\cos^3(90+\alpha) + \left(C_{15}^2 - C_{11}C_{55}\right)\cos^4(90+\alpha)\right)} \right), \quad (3)$$

where $\alpha = 40°$.

[7] The rectangular parallelepiped used for RUS investigation was cut from a large, optically clear, single crystal of spodumene using a low-speed diamond saw and polished on diamond discs (mesh 600 and 1200). The parent crystal was not the same as used to prepare the cylinders for high-pressure measurements, but it had the same characteristics of color and gem quality. Orientation was controlled by Laue diffraction, with edges parallel to **a***, [010], [001], and dimensions 7.069 × 6.501 × 6.649 mm. Deviations from the ideal orientation were less than 0.6° and opposite faces were parallel to within ±1 μm. A measure of the quality of the sample with respect to geometrical errors is provided by the difference between the density, ρ_b, obtained by the buoyancy method in pure water and the geometric density, $\rho_g = M/l_1l_2l_3$, calculated from sample mass M and dimensions l_i. These densities, $\rho_b = 3.182$ g cm^{-3} and $\rho_g = 3.173$ g cm^{-3}, agree within 0.3%.

2.3. RUS Spectroscopy

[8] The elastic constants at room temperature and atmospheric pressure were derived from the eigenfrequencies of a freely vibrating rectangular parallelepiped [*Migliori et al.*, 2001; J. Schreuer, Resonant ultrasound spectroscopy—A powerful tool for the exploration of elastic and piezoelectric properties of crystals, submitted to *Zeitschrift für Kristallographie*, 2005], using an RUS system built in house. Four resonance spectra were collected in the frequency range 300–1560 kHz, with the sample mounted in different orientations. The mechanical load on the sample was kept below 0.03 N. A total of 155 resonance frequencies was extracted from the spectra. These were used in a nonlinear least squares refinement that minimizes the quantity

$$\chi = \sum_{i=1}^{n} w_i\left(\omega_i^2(calc) - \omega_i^2(obs)\right)^2, \quad (4)$$

for n circular eigenfrequencies ω_i by adjusting the elastic constants C_{ik} of the sample, with w_i as weights calculated from experimental errors of ± 0.1 kHz in the determination of the resonance frequencies. The ω_i depend on sample orientation, shape and size as well as on mass, density and elastic constants.

[9] In each cycle of refinement the resonance frequencies of the sample for the current set of C_{ik} was calculated by solving a general eigenproblem, the rank of which equals the number of basis functions used. In order to minimize errors due to truncation effects and due to the limited precision of floating point numbers, 5313 normalized

Legendre polynomials were used for the development of the components of the displacement vector. The initial set of elastic constants was derived by modifying the literature data for diopside [*Levien et al.*, 1979] to fit the expected mean elastic stiffness of spodumene [*Haussühl*, 1993]. The final refinement yielded values for the elastic constants as listed in Table 2 for conventional reference axes. A final conversion to values for the reference system used here to analyze the $C2/c \leftrightarrow P2_1/c$ transition was achieved by applying a transformation matrix

$$\begin{bmatrix} \cos\theta & 0 & -\sin\theta \\ 0 & 1 & 0 \\ \sin\theta & 0 & \cos\theta \end{bmatrix}$$

in the normal manner for a fourth rank tensor property. A value of $\theta = 20.187°$ was used, based on $\beta = 110.187°$ reported for spodumene at room pressure and temperature by *Arlt and Angel* [2000a].

2.4. Ultrasonic Interferometry

[10] Details of the technique used to perform in situ acoustic measurements at high pressures can be found in the works of *Li et al.* [1996, 2002; see also *Liebermann and Li*, 1998; *Decremps et al.*, 2001; *Darling et al.*, 2004]. High pressures are achieved using a modified 1000 ton uniaxial split cylinder apparatus (USCA-1000) of the Kawai type. A cylindrically shaped sample rests inside the pressure medium, which, in turn, fills the octahedral cavity between corner-truncated WC cubes in a Walker-type module. A lead sleeve surrounds the sample in order to provide pseudohydrostatic pressure conditions. Pyrophyllite is chosen as the octahedral pressure medium for its good mechanical properties during cold pressurization. Changes in the electrical resistance due to two phase transitions in a piece of bismuth are used to determine pressure close to the sample in each run. Acoustic waves are generated at a $LiNbO_3$ transducer mounted on the external, truncated corner of one of the WC cubes. They travel through the WC cube (cube edge length: 25.4 mm, truncation edge length: 8 mm), an alumina buffer rod, and then the sample. Partial reflection occurs at the WC/buffer rod and the buffer rod/sample interfaces. The acoustic path ends at the interface of the sample with a Teflon insert. Gold foil, 2 μm thick, is used as a bond material to improve acoustic coupling at interfaces. Figure 1 shows a schematic cross section of the octahedron used in the present study. The setup for acoustic measurements at ambient conditions was much simpler, involving only the sample, buffer rod and transducer. Semiliquid GPA (1:1 mixture of glycerol and phthalic anhydride), 0.3 μm thick, was used as bond material and the acoustic path ended at a sample/air interface. All surfaces of the interfaces along the acoustic path, i.e., both ends of the sample cylinders and buffer rods as well as two opposite corners of a WC cube were polished to 1 μm finish.

[11] The transducer used in the experiments was for 50 MHz, P waves. For both high-pressure and ambient condition measurements, the transfer function was recorded, covering a frequency passband from 20 to 60 MHz. Pulse-echo overlap measurements were simulated offline, using carrier frequencies of 40, 50, and 60 MHz and sine tone bursts of 8 cycles as well as 5 cycles in duration. The complete data analysis of the elastic properties as a function of pressure was performed using 50 MHz, 8 cycle P wave data. Contributions from reverberations of the acoustic wave within the bonding layer were subtracted from the actually measured traveltime (t), following the procedure described by *Niesler and Jackson* [1989].

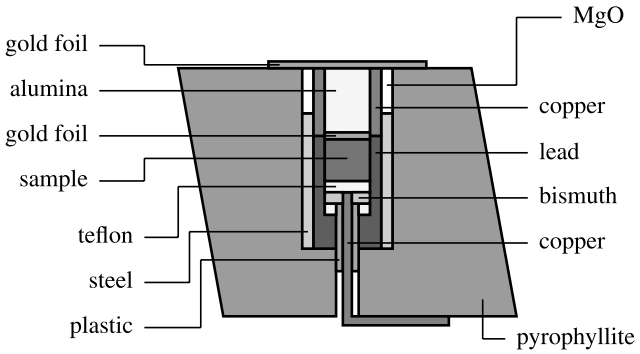

Figure 1. Cross section of the cell assembly for the high-pressure acoustic measurements.

[12] For each run, the oil pressure was typically increased slowly and continuously from 0 to 40 bars over a period of ~1.5 hours, then in 5 or 10 bar steps up to 500 bars in 5 min intervals. The transfer function was recorded at the end of each interval, averaging over a period of ~10 s. Pressure calibration was performed using the two phase transitions of Bi (Bi_I is used here to represent the $Bi_I \leftrightarrow Bi_{II}$ transition and Bi_{II} to represent the $Bi_{II} \leftrightarrow Bi_{III}$ transition). This implies a conversion of oil pressure in the press (in bars) to pressure close to the sample (in GPa), with calibration points 0, 2.55 (Bi_I) and 7.7 (Bi_{II}) GPa. A second indirect pressure calibration and quality check was achieved by monitoring traveltimes of the buffer rod for each run.

[13] Specific details of the six high-pressure runs are listed in Table 1. Sample lengths varied between 1.6 and 2.1 mm but the buffer rod was polished to a length of 3.20 ± 0.01 mm, except for run 5 in which the buffer rod length was 2.93 mm. The octahedron used in run 3 was carefully dismantled at the end of the run. Apart from a chip at one corner, which might have broken off during disassembly, the spodumene cylinder was recovered intact. The sample cylinder recovered from run 5 was also intact. It is therefore assumed that any shear stresses experienced by the crystal could only have produced strains which were below the elastic limit of the crystal.

[14] In order to determine the pressure dependence of the wave velocities and elastic constants for spodumene, the sample length (l) and density (ρ) of both the low- and high-pressure phases were calculated using the lattice parameter data of *Arlt and Angel* [2000a] and the sample length at ambient conditions. The compressional wave velocity, $v_P = 2l/t$, was calculated from the bond shift corrected traveltime (t) at a given pressure. Elastic constants were calculated using $C = \rho v_p^2$. Two runs were completed for each crystallographic direction to check the reproducibility of the results.

3. Experimental Results

3.1. RUS

[15] Table 2 lists the values of all 13 components of the elastic stiffness tensor of spodumene at ambient conditions,

based on the RUS measurements of this study, together with elastic data for spodumene and diopside from the literature. Spodumene and diopside are very similar with respect to the anisotropy of their longitudinal elastic stiffness, but spodumene is stiffer in that it has a bulk modulus which is ~35% larger than the bulk modulus of diopside (Table 2). However, a large discrepancy is observed between the new RUS elastic constants of spodumene and those reported by *Aleksandrov and Prodaivoda* [1993]. A more detailed comparison is achieved by focusing on scalar invariants of the elasticity tensor, such as the bulk modulus and the mean elastic stiffness, because the setting used by Aleksandrov and Prodaivoda is not clear. The bulk moduli in Table 2 show that their specimen was significantly softer. The difference between the elastic behavior of the two samples becomes even more evident if the elastic S values are compared, where S is the product of the mean elastic stiffness C (= $(C_{11} + C_{22} + C_{33} + C_{44} + C_{55} + C_{66} + C_{12} + C_{13} + C_{23})/9$) and the molecular volume V_M. According to *Haussühl* [1993] the S values of mainly ionic crystals can be decomposed in additive contributions $S(X_i)$ of chemically stable constituents X_i of the compound X. Taking the elastic data for Li_2O, corundum and coesite from *Nelson* [1992], $S(LiAlSi_2O_6) \approx (1/2)S(Li_2O) + (1/2)S(Al_2O_3) + 2S(\text{coesite}) = 1468 \times 10^{-20}$ Nm, in excellent agreement with the RUS value of 1423×10^{-20} Nm. The S value of Aleksandrov's specimen is much smaller and close to the experimental S value of diopside.

[16] Excellent agreement is apparent between the value of the single-crystal bulk modulus (average of K_{Reuss} and K_{Voigt}) from the RUS elastic constants, 145.0 GPa, and the value obtained from static measurements of compressibility in a diamond anvil cell, 144.2 ± 1.2 GPa [*Arlt and Angel*, 2000a]. The RUS technique is known to provide sets of elastic constants with high internal consistency [*Schreuer*, 2002], and the data presented here are believed also to have good precision and accuracy. This set of RUS parameters gives C_A = 296.1, C_B = 230.7, C_C = 279.9 GPa (1–3). Pulse-echo values determined at ambient conditions are C_A = 296.9 and 294.8 GPa (runs 1 and 2), C_B = 227.9 and 230.3 GPa (runs 3 and 4) and C_C = 274.8 GPa (run 6). The results of the high-pressure runs can be extrapolated back to zero pressure, yielding C_A = 289.8 and 292.4 GPa (runs 1 and 2), C_B = 237.2 and 235.2 GPa (runs 3 and 4) and C_C = 282.7 and 279.7 GPa (runs 5 and 6). Agreement is sufficiently close to imply that the methodology used for measuring the acoustic velocities at high pressures was robust.

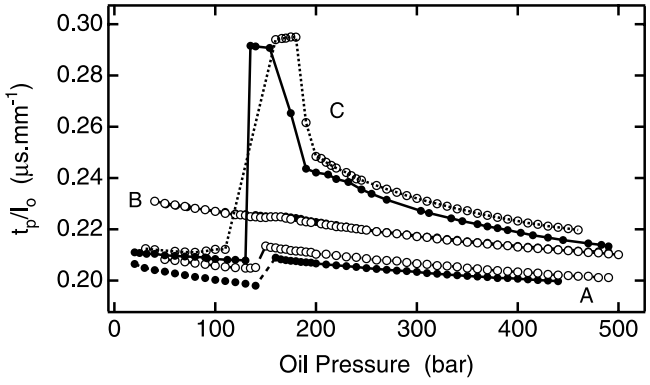

Figure 2. Reduced traveltimes (observed traveltime/sample length at ambient pressure) as a function of oil pressure through the sample: raw data, no pressure calibration, and no bond shift correction.

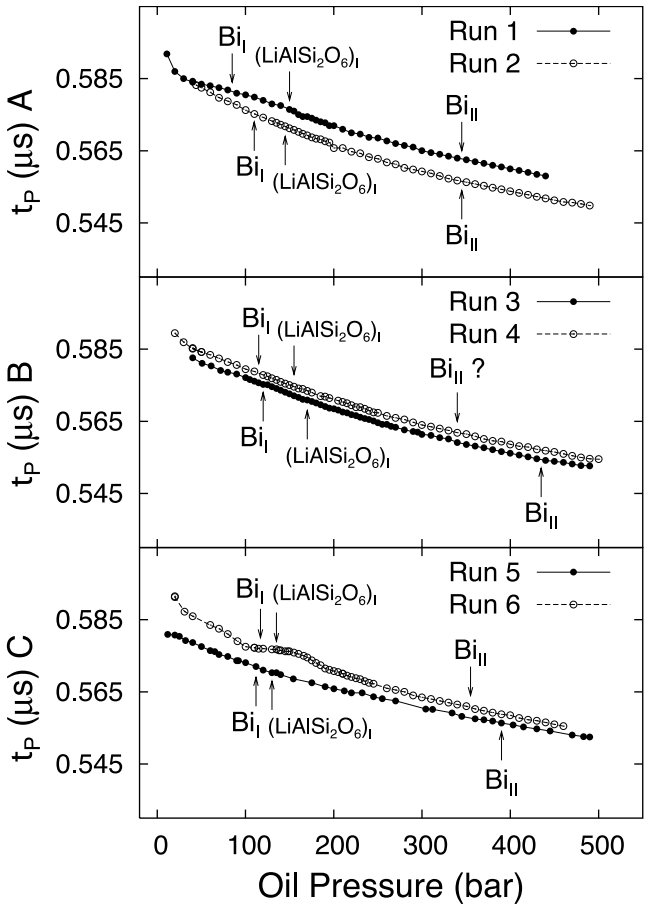

Figure 3. Traveltimes as a function of oil pressure through the buffer rod: raw data, no pressure calibration, and no bond shift correction. The transition points of Bi (Bi_I, Bi_{II}) from electrical measurements and of $LiAlSi_2O_6$ $(LiAlSi_2O_6)_I$ from anomalies in the traveltimes are also indicated.

3.2. Ultrasonic Interferometry

[17] Complete sets of experimental data are given for each run in Tables S1–S6 of the auxiliary material[1]. Figure 2 shows the traveltimes (t_P) for the samples, with respect to the sample length at ambient conditions (l_o). Immediately evident in the raw data are significant discontinuities in traveltimes for the A and C directions at ~120–170 bars oil pressure. Traveltimes for the B direction show a cusp within the same range. These anomalies are interpreted as being due to the displacive transition, which occurs at ~3.19 GPa according to *Arlt and Angel* [2000a]. Use of the pressure calibration from the transitions in bismuth placed the sharp

[1]Auxiliary material is available at ftp://ftp.agu.org/apend/jb/2005jb004098.

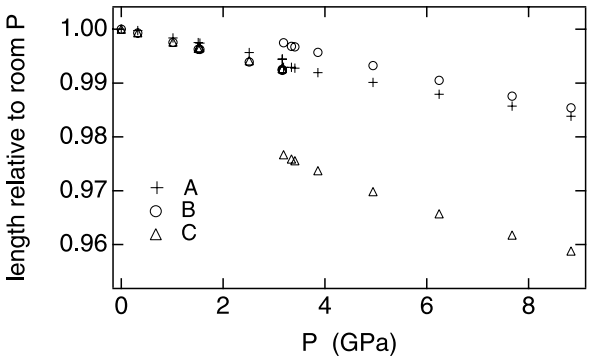

Figure 4. Relative changes in linear dimension as a function of pressure for the three directions, A, B, and C, calculated from the lattice parameter data of *Arlt and Angel* [2000a].

step in traveltimes for A and C directions at absolute pressures of 2.9–4.2 GPa (Table 1). The pressure calibration was further refined by using the traveltimes for the alumina buffer rod. These traveltimes varied smoothly with oil pressure in runs 2–5 (Figure 3) and can be described by a second-order polynomial. A three-point pressure calibration using Bi should yield quite reliable values for pressure near the sample, therefore. For run numbers 1 and 6 the buffer rod traveltimes varied less smoothly as a function of oil pressure below ~200 bars (Figure 3). In these two cases, a more reliable pressure calibration was obtained by comparing the buffer rod traveltimes with those of a 'good' run, i.e., run 3. The resulting transition pressures appear to be slightly lower for direction C, in comparison with the other two directions, but the variations could also be due simply to experimental scatter.

[18] In order to progress from traveltimes to calculated elastic constants, it was necessary to put all the data onto the same pressure scale as the single-crystal data of *Arlt and Angel* [2000a]. The discontinuity in traveltimes closest to their transition pressure (3.19 GPa) was obtained from run 3 (3.17 GPa). This run also yielded a smooth relationship between buffer rod traveltimes and oil pressure. It was therefore assumed that the buffer rod traveltimes for this run could themselves be used to give calibration of pressure for the other runs with more internal consistency than was given by the Bi_I and Bi_{II} transition points alone. The calibration curves were also shifted to ensure that the spodumene transition point ended up at 3.19 GPa in each case.

[19] The lattice parameter data of *Arlt and Angel* [2000a] were used to calculate linear strains for each of the directions A, B and C. These are shown in Figure 4 relative to values of unity at room pressure. A simple 3 parameter polynomial was used to fit the data for pressure intervals above and below 3.19 GPa in order to calculate sample lengths as a function of pressure. The fits were then used for calculating the traveltimes through each sample, and Figure 5 shows the resulting acoustic P wave velocities. Finally, density variations calculated from the unit cell volume data of *Arlt and Angel* [2000a] (Figure 4) were used to convert velocities to elastic constants and the resulting variations of C_A, C_B and C_C are shown in Figure 6. The data in Figures 5 and 6 have been reduced by applying pressure calibrations, based on Bi reference points and buffer rod traveltimes, and corrected for reverberations within the bonding layer. While this procedure still leaves some scatter in the experimental data, it does not alter the distinctive features which can be associated with the phase transition in spodumene. The abrupt discontinuity in C_A and C_C with increasing pressure is interpreted as marking the onset of the transition. This is followed by an increase in stiffness, though for C_C there is a range of ~0.5–1 GPa over which the values remain low. C_B shows a much smaller anomaly. Reproducibility of the measurements is best for C_B, as would be expected also from inspection of the smooth variations of buffer rod traveltimes for these two runs (3 and 4). Discrepancies in the absolute values of the results for runs 1 and 6, in comparison with runs 2 and 5, can probably be attributed to displacements of some of the components in the octahedron during pressurization. Runs 2 and 5 are judged to give the most reliable values of C_A and C_C at high pressures on the basis that their

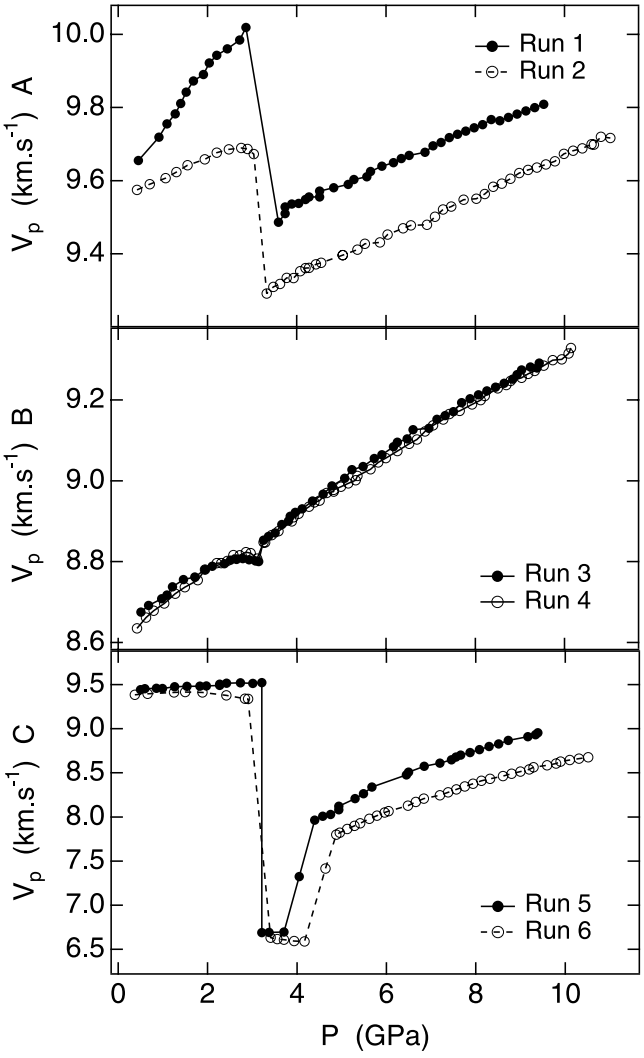

Figure 5. Acoustic velocities as a function of pressure: pressure calibrated and bond shift corrected.

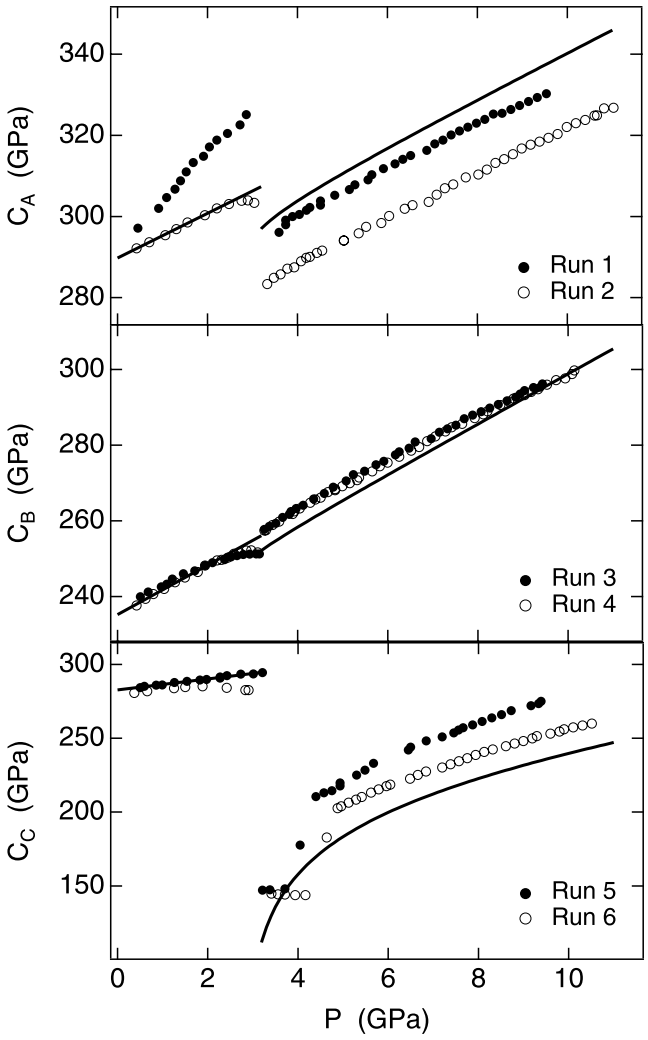

Figure 6. Elastic constants as a function of pressure: pressure calibrated and bond shift corrected. Linear fits shown for the experimental data below 3.19 GPa, ignoring softening ahead of the transition, gave $C_A^o = 289.8 + 5.51\ P$, $C_B^o = 235.2 + 6.53\ P$, and $C_C^o = 282.7 + 3.72\ P$ GPa. Curves above 3.19 GPa are Landau solutions for the softening of C_A, C_B, and C_C subtracted from extrapolations of the linear fits to the low pressure data for $C2/c$ crystals.

buffer rod traveltimes show the same smooth variation with oil pressure as found for runs 3 and 4 (Figure 3).

[20] The first sample echo was also examined with respect to amplitude in order to provide an approximate measure of changes in attenuation through the phase transition. Variations of the ratio of the amplitude of the sample echo with respect to the amplitude of the first buffer rod echo at each pressure are shown in Figure 7. In all the runs, apart from run 2, this amplitude ratio decreased with increasing pressure. The spodumene transition is marked by a distinct drop in amplitude (increase in attenuation) for the A and B directions. For the C direction, the same drop in amplitude is observed near the transition point but recovery is spread over a wider pressure interval in the $P2_1/c$ stability field.

4. Landau Theory

[21] The active representation for the $C2/c \leftrightarrow P2_1/c$ transition is Y_2^-. A Landau expansion for the excess free energy, to sixth order in Q and to lowest order in strain/order parameter coupling terms, is

$$G = \frac{1}{2}a(P - P_c)Q^2 + \frac{1}{4}bQ^4 + \frac{1}{6}cQ^6 + \lambda_1 e_1 Q^2 + \lambda_2 e_2 Q^2 + \lambda_3 e_3 Q^2 + \lambda_4 e_4^2 Q^2 + \lambda_5 e_5 Q^2 + \lambda_6 e_6^2 Q^2 + \frac{1}{2}\sum_{i,k} C_{ik}^o e_i e_k. \quad (5)$$

Here e_1-e_6 are strain components, a, b, c are normal Landau coefficients, λ_i are strain/order parameter coupling coefficients, P is pressure, P_c is the critical pressure, and C_{ik}^o are elastic constants of the high-symmetry ($C2/c$) phase (usually referred to as the bare elastic constants). Setting the

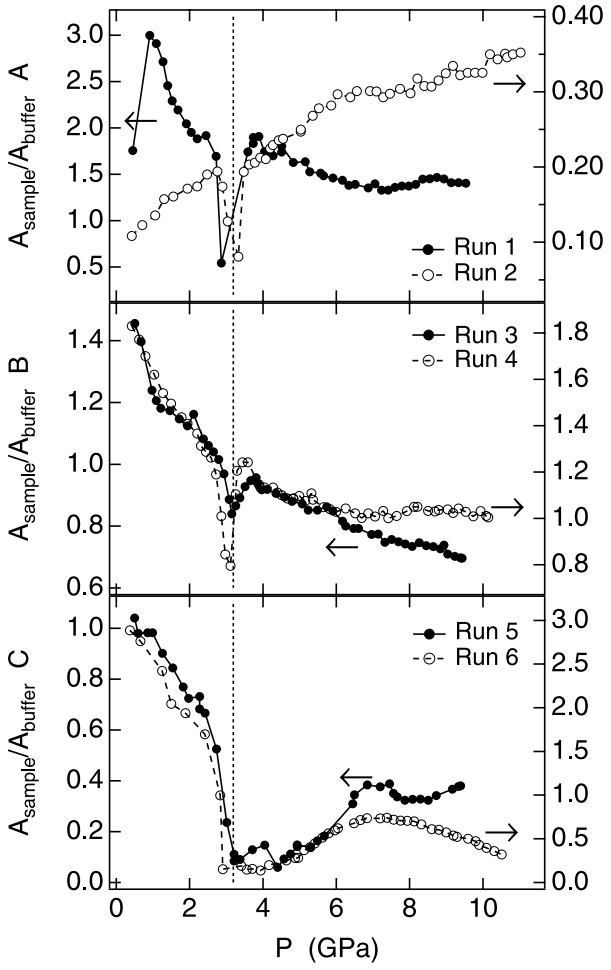

Figure 7. Ratio of amplitudes A_{sample}/A_{buffer} as a function of pressure: pressure calibrated.

equilibrium condition, $\partial G/\partial e_i = 0$, gives relationships between strain components and the order parameter as

$$e_1 = \frac{\begin{bmatrix} \left(C_{25}^{o2}C_{33}^{o} - 2C_{23}^{o}C_{25}^{o}C_{35}^{o} + C_{22}^{o}C_{35}^{o2} + C_{23}^{o2}C_{55}^{o} - C_{22}^{o}C_{33}^{o}C_{55}^{o}\right)\lambda_1 \\ +\left(-C_{15}^{o}C_{25}^{o}C_{33}^{o} + C_{15}^{o}C_{23}^{o}C_{35}^{o} + C_{13}^{o}C_{25}^{o}C_{35}^{o} - C_{12}^{o}C_{35}^{o2} - C_{13}^{o}C_{23}^{o}C_{55}^{o} + C_{12}^{o}C_{33}^{o}C_{55}^{o}\right)\lambda_2 \\ +\left(C_{15}^{o}C_{23}^{o}C_{25}^{o} - C_{13}^{o}C_{25}^{o2} - C_{15}^{o}C_{22}^{o}C_{35}^{o} + C_{12}^{o}C_{25}^{o}C_{35}^{o} + C_{13}^{o}C_{22}^{o}C_{55}^{o} - C_{12}^{o}C_{23}^{o}C_{55}^{o}\right)\lambda_3 \\ +\left(-C_{15}^{o}C_{23}^{o2} + C_{13}^{o}C_{23}^{o}C_{25}^{o} + C_{15}^{o}C_{22}^{o}C_{33}^{o} - C_{12}^{o}C_{25}^{o}C_{33}^{o} - C_{13}^{o}C_{22}^{o}C_{35}^{o} + C_{12}^{o}C_{23}^{o}C_{35}^{o}\right)\lambda_5 \end{bmatrix}}{\begin{bmatrix} C_{15}^{o2}C_{23}^{o2} - 2C_{13}^{o}C_{15}^{o}C_{23}^{o}C_{25}^{o} + C_{13}^{o2}C_{25}^{o2} - C_{15}^{o2}C_{22}^{o}C_{33}^{o} + 2C_{12}^{o}C_{15}^{o}C_{25}^{o}C_{33}^{o} - C_{11}^{o}C_{25}^{o2}C_{33}^{o} \\ +2C_{13}^{o}C_{15}^{o}C_{22}^{o}C_{35}^{o} - 2C_{12}^{o}C_{15}^{o}C_{23}^{o}C_{35}^{o} - 2C_{12}^{o}C_{13}^{o}C_{25}^{o}C_{35}^{o} + 2C_{11}^{o}C_{23}^{o}C_{25}^{o}C_{35}^{o} + C_{12}^{o2}C_{35}^{o2} \\ -C_{11}^{o}C_{22}^{o}C_{35}^{o2} - C_{13}^{o2}C_{22}^{o}C_{55}^{o} + 2C_{12}^{o}C_{13}^{o}C_{23}^{o}C_{55}^{o} - C_{11}^{o}C_{23}^{o2}C_{55}^{o} - C_{12}^{o2}C_{33}^{o}C_{55}^{o} + C_{11}^{o}C_{22}^{o}C_{33}^{o}C_{55}^{o} \end{bmatrix}} Q^2 \tag{6}$$

$$e_2 = \frac{\begin{bmatrix} \left(-C_{15}^{o}C_{25}^{o}C_{33}^{o} + C_{15}^{o}C_{23}^{o}C_{35}^{o} + C_{13}^{o}C_{25}^{o}C_{35}^{o} - C_{12}^{o}C_{35}^{o2} - C_{13}^{o}C_{23}^{o}C_{55}^{o} + C_{12}^{o}C_{33}^{o}C_{55}^{o}\right)\lambda_1 \\ +\left(C_{15}^{o2}C_{33}^{o} - 2C_{13}^{o}C_{15}^{o}C_{35}^{o} + C_{11}^{o}C_{35}^{o2} + C_{13}^{o2}C_{55}^{o} - C_{11}^{o}C_{33}^{o}C_{55}^{o}\right)\lambda_2 \\ +\left(-C_{15}^{o2}C_{23}^{o} + C_{13}^{o}C_{15}^{o}C_{25}^{o} + C_{12}^{o}C_{15}^{o}C_{35}^{o} - C_{11}^{o}C_{25}^{o}C_{35}^{o} - C_{12}^{o}C_{13}^{o}C_{55}^{o} + C_{11}^{o}C_{23}^{o}C_{55}^{o}\right)\lambda_3 \\ +\left(C_{13}^{o}C_{15}^{o}C_{23}^{o} - C_{13}^{o2}C_{25}^{o} - C_{12}^{o}C_{15}^{o}C_{33}^{o} + C_{11}^{o}C_{25}^{o}C_{33}^{o} + C_{12}^{o}C_{13}^{o}C_{35}^{o} - C_{11}^{o}C_{23}^{o}C_{35}^{o}\right)\lambda_5 \end{bmatrix}}{\begin{bmatrix} C_{15}^{o2}C_{23}^{o2} - 2C_{13}^{o}C_{15}^{o}C_{23}^{o}C_{25}^{o} + C_{13}^{o2}C_{25}^{o2} - C_{15}^{o2}C_{22}^{o}C_{33}^{o} + 2C_{12}^{o}C_{15}^{o}C_{25}^{o}C_{33}^{o} - C_{11}^{o}C_{25}^{o2}C_{33}^{o} \\ +2C_{13}^{o}C_{15}^{o}C_{22}^{o}C_{35}^{o} - 2C_{12}^{o}C_{15}^{o}C_{23}^{o}C_{35}^{o} - 2C_{12}^{o}C_{13}^{o}C_{25}^{o}C_{35}^{o} + 2C_{11}^{o}C_{23}^{o}C_{25}^{o}C_{35}^{o} + C_{12}^{o2}C_{35}^{o2} \\ -C_{11}^{o}C_{22}^{o}C_{35}^{o2} - C_{13}^{o2}C_{22}^{o}C_{55}^{o} + 2C_{12}^{o}C_{13}^{o}C_{23}^{o}C_{55}^{o} - C_{11}^{o}C_{23}^{o2}C_{55}^{o} - C_{12}^{o2}C_{33}^{o}C_{55}^{o} + C_{11}^{o}C_{22}^{o}C_{33}^{o}C_{55}^{o} \end{bmatrix}} Q^2 \tag{7}$$

$$e_3 = \frac{\begin{bmatrix} \left(C_{15}^{o}C_{23}^{o}C_{25}^{o} - C_{13}^{o}C_{25}^{o2} - C_{15}^{o}C_{22}^{o}C_{35}^{o} + C_{12}^{o}C_{25}^{o}C_{35}^{o} + C_{13}^{o}C_{22}^{o}C_{55}^{o} - C_{12}^{o}C_{23}^{o}C_{55}^{o}\right)\lambda_1 \\ +\left(-C_{15}^{o2}C_{23}^{o} + C_{13}^{o}C_{15}^{o}C_{25}^{o} + C_{12}^{o}C_{15}^{o}C_{35}^{o} - C_{11}^{o}C_{25}^{o}C_{35}^{o} - C_{12}^{o}C_{13}^{o}C_{55}^{o} + C_{11}^{o}C_{23}^{o}C_{55}^{o}\right)\lambda_2 \\ +\left(C_{15}^{o2}C_{22}^{o} - 2C_{12}^{o}C_{15}^{o}C_{25}^{o} + C_{11}^{o}C_{25}^{o2} + C_{12}^{o2}C_{55}^{o} - C_{11}^{o}C_{22}^{o}C_{55}^{o}\right)\lambda_3 \\ +\left(-C_{13}^{o}C_{15}^{o}C_{22}^{o} + C_{12}^{o}C_{15}^{o}C_{23}^{o} + C_{12}^{o}C_{13}^{o}C_{25}^{o} - C_{11}^{o}C_{23}^{o}C_{25}^{o} - C_{12}^{o2}C_{35}^{o} + C_{11}^{o}C_{22}^{o}C_{35}^{o}\right)\lambda_5 \end{bmatrix}}{\begin{bmatrix} C_{15}^{o2}C_{23}^{o2} - 2C_{13}^{o}C_{15}^{o}C_{23}^{o}C_{25}^{o} + C_{13}^{o2}C_{25}^{o2} - C_{15}^{o2}C_{22}^{o}C_{33}^{o} + 2C_{12}^{o}C_{15}^{o}C_{25}^{o}C_{33}^{o} - C_{11}^{o}C_{25}^{o2}C_{33}^{o} \\ +2C_{13}^{o}C_{15}^{o}C_{22}^{o}C_{35}^{o} - 2C_{12}^{o}C_{15}^{o}C_{23}^{o}C_{35}^{o} - 2C_{12}^{o}C_{13}^{o}C_{25}^{o}C_{35}^{o} + 2C_{11}^{o}C_{23}^{o}C_{25}^{o}C_{35}^{o} + C_{12}^{o2}C_{35}^{o2} \\ -C_{11}^{o}C_{22}^{o}C_{35}^{o2} - C_{13}^{o2}C_{22}^{o}C_{55}^{o} + 2C_{12}^{o}C_{13}^{o}C_{23}^{o}C_{55}^{o} - C_{11}^{o}C_{23}^{o2}C_{55}^{o} - C_{12}^{o2}C_{33}^{o}C_{55}^{o} + C_{11}^{o}C_{22}^{o}C_{33}^{o}C_{55}^{o} \end{bmatrix}} Q^2 \tag{8}$$

$$e_5 = \frac{\begin{bmatrix} \left(-C_{15}^{o}C_{23}^{o2} + C_{13}^{o}C_{23}^{o}C_{25}^{o} + C_{15}^{o}C_{22}^{o}C_{33}^{o} - C_{12}^{o}C_{25}^{o}C_{33}^{o} - C_{13}^{o}C_{22}^{o}C_{35}^{o} + C_{12}^{o}C_{23}^{o}C_{35}^{o}\right)\lambda_1 \\ +\left(C_{13}^{o}C_{15}^{o}C_{23}^{o} - C_{13}^{o2}C_{25}^{o} - C_{12}^{o}C_{15}^{o}C_{33}^{o} + C_{11}^{o}C_{25}^{o}C_{33}^{o} + C_{12}^{o}C_{13}^{o}C_{35}^{o} - C_{11}^{o}C_{23}^{o}C_{35}^{o}\right)\lambda_2 \\ +\left(-C_{13}^{o}C_{15}^{o}C_{22}^{o} + C_{12}^{o}C_{15}^{o}C_{23}^{o} + C_{12}^{o}C_{13}^{o}C_{25}^{o} - C_{11}^{o}C_{23}^{o}C_{25}^{o} - C_{12}^{o2}C_{35}^{o} + C_{11}^{o}C_{22}^{o}C_{35}^{o}\right)\lambda_3 \\ +\left(C_{13}^{o2}C_{22}^{o} - 2C_{12}^{o}C_{13}^{o}C_{23}^{o} + C_{11}^{o}C_{23}^{o2} + C_{12}^{o2}C_{33}^{o} - C_{11}^{o}C_{22}^{o}C_{33}^{o}\right)\lambda_5 \end{bmatrix}}{\begin{bmatrix} C_{15}^{o2}C_{23}^{o2} - 2C_{13}^{o}C_{15}^{o}C_{23}^{o}C_{25}^{o} + C_{13}^{o2}C_{25}^{o2} - C_{15}^{o2}C_{22}^{o}C_{33}^{o} + 2C_{12}^{o}C_{15}^{o}C_{25}^{o}C_{33}^{o} - C_{11}^{o}C_{25}^{o2}C_{33}^{o} \\ +2C_{13}^{o}C_{15}^{o}C_{22}^{o}C_{35}^{o} - 2C_{12}^{o}C_{15}^{o}C_{23}^{o}C_{35}^{o} - 2C_{12}^{o}C_{13}^{o}C_{25}^{o}C_{35}^{o} + 2C_{11}^{o}C_{23}^{o}C_{25}^{o}C_{35}^{o} + C_{12}^{o2}C_{35}^{o2} \\ -C_{11}^{o}C_{22}^{o}C_{35}^{o2} - C_{13}^{o2}C_{22}^{o}C_{55}^{o} + 2C_{12}^{o}C_{13}^{o}C_{23}^{o}C_{55}^{o} - C_{11}^{o}C_{23}^{o2}C_{55}^{o} - C_{12}^{o2}C_{33}^{o}C_{55}^{o} + C_{11}^{o}C_{22}^{o}C_{33}^{o}C_{55}^{o} \end{bmatrix}} Q^2, \tag{9}$$

with $e_4 = e_6 = 0$. Substituting these back into Equation 5 gives the renormalized expansion

$$G = \frac{1}{2}a(P - P_c)Q^2 + \frac{1}{4}b^* Q^4 + \frac{1}{6}cQ^6 \quad (10)$$

where

$$b^* = b + f\left(\lambda_1, \lambda_2, \lambda_3, \lambda_5, C_{11}^o, C_{22}^o, C_{33}^o, C_{12}^o, C_{13}^o, C_{23}^o, C_{55}^o, C_{15}^o, C_{25}^o, C_{35}^o\right). \quad (11)$$

The function in brackets contains a large number of terms and is not given here, therefore. All the algebraic manipulations required were accomplished using the software package Mathematica.

[22] The transition is first order in character [*Arlt and Angel*, 2000a] and therefore has $b^* < 0$. In this case the evolution of the equilibrium order parameter is given by the standard solution

$$Q^2 = \frac{2}{3}Q_o^2\left\{1 + \left[1 - \frac{3}{4}\left(\frac{P - P_c}{P_{tr} - P_c}\right)\right]^{1/2}\right\}, \quad (12)$$

and there is a step in the value of Q from 0 to Q_o at the transition pressure, P_{tr}, where

$$Q_o^2 = -\frac{4a}{b^*}(P_{tr} - P_c). \quad (13)$$

Another useful relationship is

$$P_{tr} = P_c + \frac{3b^{*2}}{16ac}. \quad (14)$$

[23] Following *Slonczewski and Thomas* [1970] the elastic constants, C_{ik}, of the $P2_1/c$ structure are given by

$$C_{ik} = C_{ik}^o - \frac{\partial^2 G}{\partial e_i \partial Q}\cdot\left(\frac{\partial^2 G}{\partial Q^2}\right)^{-1}\cdot\frac{\partial^2 G}{\partial e_k \partial Q} \quad (15)$$

and, hence

$$C_{11} = C_{11}^o - 4\lambda_1^2 Q^2\chi \quad (16)$$

$$C_{22} = C_{22}^o - 4\lambda_2^2 Q^2\chi \quad (17)$$

$$C_{33} = C_{33}^o - 4\lambda_3^2 Q^2\chi \quad (18)$$

$$C_{12} = C_{12}^o - 4\lambda_1\lambda_2 Q^2\chi \quad (19)$$

$$C_{13} = C_{13}^o - 4\lambda_1\lambda_3 Q^2\chi \quad (20)$$

$$C_{23} = C_{23}^o - 4\lambda_2\lambda_3 Q^2\chi \quad (21)$$

$$C_{55} = C_{55}^o - 4\lambda_5^2 Q^2\chi \quad (22)$$

$$C_{15} = C_{15}^o - 4\lambda_1\lambda_5 Q^2\chi \quad (23)$$

$$C_{25} = C_{25}^o - 4\lambda_2\lambda_5 Q^2\chi \quad (24)$$

$$C_{35} = C_{35}^o - 4\lambda_3\lambda_5 Q^2\chi. \quad (25)$$

The inverse order parameter susceptibility, χ^{-1}, is

$$\chi^{-1} = \frac{\partial^2 G}{\partial Q^2} = a(P - P_c) + (2b + b^*)Q^2 + 5cQ^4. \quad (26)$$

Coupling of the form $\lambda e^2 Q^2$ leads to

$$C_{44} = C_{44}^o + 2\lambda_4 Q^2 \quad (27)$$

$$C_{66} = C_{66}^o + 2\lambda_6 Q^2 \quad (28)$$

$$C_{46} = C_{46}^o + \sqrt{\lambda_4\lambda_6}Q^2. \quad (29)$$

5. Pressure Dependence of the Equilibrium Order Parameter and Evaluation of Strain Parameters

[24] *Arlt and Angel* [2000a] found that the intensities of superlattice reflections (I_b, $h+k$ = odd) in single-crystal X-ray diffraction patterns give an internally consistent picture of the evolution of the $P2_1/c$ structure at high pressures in each of spodumene, $LiScSi_2O_6$, and $ZnSiO_3$. Their data for $(I_{23\bar{3}} + I_{30\bar{4}} + I_{70\bar{4}})$ of spodumene, scaled with respect to the intensity of a sublattice reflection ($I_a = I_{223}$), are reproduced in Figure 8a. Following the normal expectation that I_b/I_a should scale with Q^2, (12) can be given as

$$\frac{I_b}{I_a} \propto \left\{1 + \left[1 - \frac{3}{4}\left(\frac{P - P_c}{P_{tr-P_c}}\right)\right]^{1/2}\right\}. \quad (30)$$

Equation (30) has been fit to the intensity data at $P > 3.2$ GPa, giving $P_c = 4.01$ GPa for P_{tr} fixed at 3.19 GPa (Figure 8a). For transitions driven by temperature as the external variable, absolute values of the order parameter are usually defined with respect to $Q = 1$ at 0 K. There is no equivalent constraint for pressure, and the scaling of Q is a matter for arbitrary choice so long as $Q < 1$ is maintained over the pressure range of interest. $Q_o = 0.2$ has been chosen here. This allows the variation of Q to be calculated for all pressures above 3.19 GPa.

[25] *Arlt and Angel* [2000a] also found an unusual pattern of evolution for the spontaneous strains (reproduced in Figure 8b). These are all expected to scale with Q^2 (6–9) but e_1 and e_2, in particular, have a quite different evolution from the others (Figure 8c). In general, there are three straightforward explanations for strain evolution which differs from simple predicted relationships of this type. First, there is always some inherent uncertainty in the extrapolation of reference lattice parameters to high pressures. Arlt and Angel used an equation of state of the form

$$l_o = l'_o\left[1 + \frac{K'}{K_o}P\right]^{-\frac{1}{3K'}} \quad (31)$$

to make this extrapolation. Here l_o is a lattice parameter (a_o, b_o or c_o) of the $C2/c$ structure and l'_o is the value at zero pressure. K_o is an elastic constant and K' its pressure dependence. They assumed $K' = 4$ when obtaining fits for a_o, b_o or c_o. Alternative choices of values, such as $K' = 5$ or 6, make only small differences to the strains which are determined from the lattice parameters.

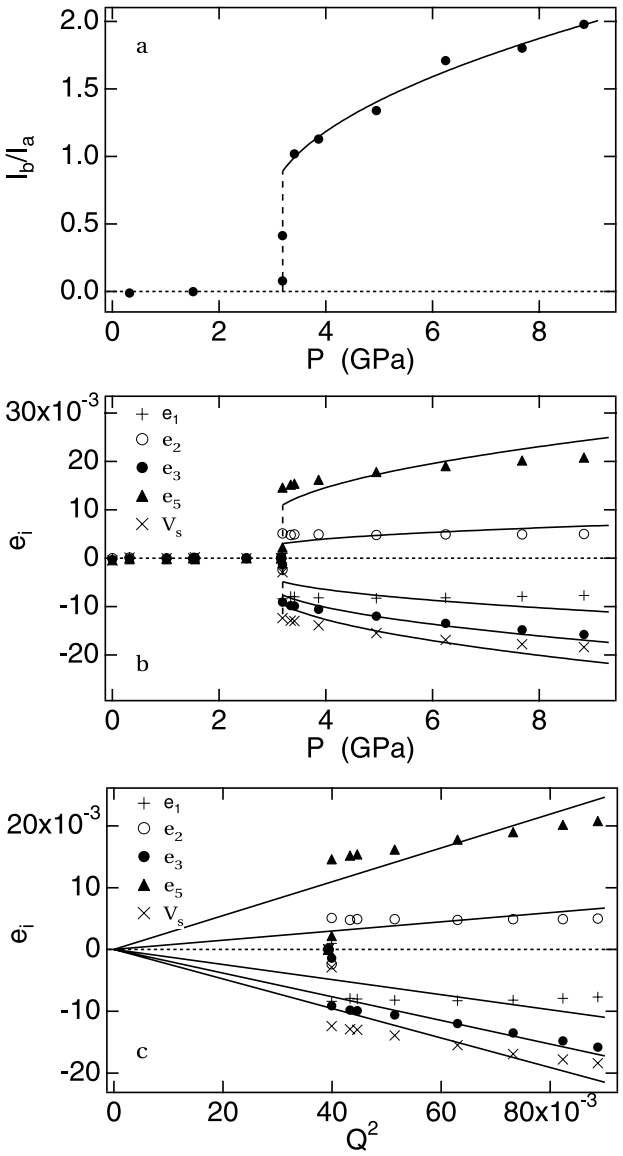

Figure 8. (a) Variations of the sum of intensities of selected $h+k$ = odd reflections, scaled with respect to an $h+k$ = even reflection (I_b/I_a). Data are from *Arlt and Angel* [2000a]. The curve is a fit of (30) to the data, with P_{tr} fixed at 3.19 GPa. (b) Variations of strain determined using lattice parameter data of *Arlt and Angel* [2000a]. Curves are parameterizations of the strains based on the linear fits shown in Figure 8c. The curve for V_s is the sum of the paramaterized variations $e_1 + e_2 + e_3$. (c) Linear fits to the strains of *Arlt and Angel* [2000a] with respect to Q^2.

[26] A second source of anomalous variations from classical strain evolution can be attributed to pressure dependence of the bare elastic constants. For example, the volume strain, V_s, would normally be expected to evolve with Q^2 as

$$V_s = \frac{-\lambda_v}{(K_o + K'P)^o} Q^2 \tag{32}$$

where λ_v is the coefficient for coupling between the volume strain and the driving order parameter, and the superscript ^{o} signifies the (pressure-dependent) bulk modulus of the $C2/c$ structure. For a constant value of λ_v, the true variation of Q^2 is thus expected to scale with $V_s\,(K_o + K'P)^o$. This treatment could lead to a better match with the observed strains but data for the pressure dependence of all the bare elastic constants are needed in order to take it further.

[27] A third possible explanation for anomalous strain evolution is that the coupling coefficients are pressure-dependent or that there are contributions from higher-order strain/order parameter couplings. It is not easy to distinguish between these two effects but, although more than one coupling term is rarely required for a given strain, higher-order coupling effects have been observed in a small number of systems [*Carpenter et al.*, 1998a]. In the present case, the next coupling terms permitted by symmetry in (5) are $\lambda'_1 e_1 Q^4 + \lambda'_2 e_2 Q^4 + \lambda'_3 e_3 Q^4$. Their inclusion would lead to strain relationships of the form $e = AQ^2 + BQ^4$, as in the case of quartz [*Carpenter et al.*, 1998b]. The strain variations in Figures 8b and 8c can indeed be described by a function of this form but some preliminary calculations suggested that they would not then lead to a match with the observed elastic constant variations. Other possible higher-order terms include $\lambda'_1 e_1^2 Q^2 + \lambda'_2 e_2^2 Q^2 + \lambda'_3 e_3^2 Q^2$. These can be thought of as renormalizing the elastic constants such that C_{11}^o becomes $(C_{11}^o + 2\lambda'_1 Q^2)$, C_{22}^o becomes $(C_{22}^o + 2\lambda'_2 Q^2)$, etc.

[28] In the absence of data for the pressure dependence of most of the elastic constants of $C2/c$ spodumene, the simplest model for representing the strain evolution remains that given by (5)–(9). Linear fits to each of e_1, e_2, e_3 and e_5 from *Arlt and Angel* [2000a] with respect to Q^2 (for Q_o = 0.2, P_{tr} = 3.19 GPa, P_c = 4.01 GPa) are shown in Figure 8c. These fits have been used to find values for the coupling coefficients: λ_1 = 30.9, λ_2 = 11.4, λ_3 = 64.5, λ_5 = −26.4 GPa. As seen in Figure 8b, these solutions only represent the true variations of the strains semiquantitatively. The fit to V_s in Figure 8c gives λ_v = 34.4 GPa, from (32) with a fixed value of K^o = 144.2 GPa.

6. Elastic Constant Variations

[29] In order to calculate the equilibrium variation of C_A, C_B and C_C in the $P2_1/c$ stability field, it is necessary to obtain values for four remaining parameters, a, b, b^* and c in (26). A value of $b - b^*$ = 45.0 GPa is obtained by substituting values for the coupling coefficients and the bare elastic constants (Table 3) into (11). The ratio a/b^* is given by (13), and an additional relationship between a, b^* and c

Table 3. Values of Landau Parameters

Landau Parameters	Bare Elastic Constants
P_{tr} = 3.19 GPa	C_{11}^o = 233 GPa
P_c = 4.01 GPa	C_{22}^o = 231
a = −0.5	C_{33}^o = 290
b = 4.0 GPa	C_{44}^o = 103
b^* = −41.0 GPa	C_{55}^o = 99
c = 769 GPa	C_{66}^o = 82
λ_1 = 30.9 GPa	C_{12}^o = 93
λ_2 = 11.4 GPa	C_{13}^o = 95
λ_3 = 64.5 GPa	C_{23}^o = 93
λ_5 = −26.4 GPa	C_{15}^o = 32
λ_4 = 100 GPa	C_{25}^o = 2
λ_6 = 100 GPa	C_{35}^o = −16
λ_v = 34.4GPa	C_{46}^o = 4

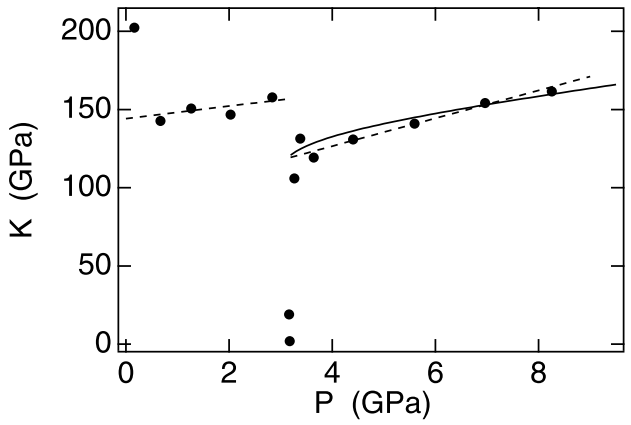

Figure 9. Bulk modulus as a function of pressure, extracted from the unit cell volume data of *Arlt and Angel* [2000a]. Dashed lines are Murnaghan equation of state fits from Arlt and Angel. Solid line is the Landau solution for the bulk modulus of $P2_1/c$ spodumene, using the Arlt and Angel fit for the $C2/c$ structure as a baseline (144.2 + 4 P GPa).

is given by (14). Only one unknown parameter remains, and this can be extracted from fitting of the bulk modulus using the data of *Arlt and Angel* [2000a] once more.

[30] Figure 9 shows the variation of bulk modulus as a function of pressure, as determined from successive pairs of data points for unit cell volume, V, as a function of P. Each adjacent pair of data points, V_1 and V_2 at P_1 and P_2, from *Arlt and Angel* [2000a] was used to calculate a value of bulk modulus equal to $-(1/2)(V_1 + V_2)(P_1 - P_2)/(V_1 - V_2)$. A simplified Landau expansion with the bulk modulus of the $C2/c$ structure and the volume strain included explicitly would be of the form

$$G = G(\mathrm{L}) + \lambda_v V_s Q^2 + \frac{1}{2} K^o V_s^2 \tag{33}$$

giving, for the $P2_1/c$ structure,

$$K = K^o - 4\lambda_v^2 Q^2 \chi. \tag{34}$$

G(L) represents the standard Landau 246 terms in Q, and K^o = 144.2 + 4P from *Arlt and Angel* [2000a]. Trial values of the a coefficient in (26), with values of b, b^* and c determined from the other relationships, were selected until the fit for K shown in Figure 9 was obtained. The full set of parameters for this solution is listed in Table 3.

[31] Variations of the individual elastic constants given by (16)–(25) were calculated using the full set of coefficients in Table 3, with constant values of the bare elastic constants, C_{ik}^o. These were then used to calculate changes expected in C_A, C_B and C_C due to the phase transition (1)–(3). Experimental data for the $C2/c$ structure at $P < P_{tr}$ were used to determine linear variations for the baseline/bare elastic constants in each of the three directions (runs 2, 4, and 5; Figure 6). The final variations of C_A, C_B and C_C for $P2_1/c$ structural states shown in Figure 6 are then the changes calculated for the phase transition subtracted from these pressure-dependent baselines as extrapolated above 3.19 GPa.

[32] Apart from baselines for the $C2/c$ structure, the calculated elastic anomalies associated with the phase transition contain no input of data from the observed anomalies. Comparison of the two is therefore a real test of the Landau model. Agreement is semiquantitative, with C_B (= C_{22}) hardly affected by the transition and the largest changes found for direction C. The form of softening is correctly reproduced, with C_C showing a large curvature in the $P2_1/c$ stability field, while C_A has a much flatter variation. However, the calculated softening of C_C is large with respect to the observed softening while the calculated softening of C_A is too small. From the equations for each of C_{11}, C_{22}, etc. ((16)–(25)), it seems likely that an alternative choice of values for the coupling coefficients, λ_1, λ_2, λ_3 and λ_5, might produce a better match with the experimental data. This suggests that the mismatch arises primarily from an imperfect representation of the individual spontaneous strains with respect to the variation of the order parameter (Figure 8).

7. Discussion

[33] The initial premise of the present study, that the $C2/c \leftrightarrow P2_1/c$ transition in pyroxenes must be accompanied by a substantial elastic anomaly, has been confirmed. The magnitudes of the anomalies calculated for C_A, C_B (= C_{22}) and C_C scale according to the observed magnitudes, even though exact matches have not been obtained. Discontinuities in C_A and C_C at the transition point are associated with large values of the strain coupling coefficients λ_1, λ_3 and λ_5. On the other hand λ_2 is smaller and the anomaly in C_{22} correspondingly less. If the slight stiffening observed in C_{22} for $P2_1/c$ with respect to the $C2/c$ structure is correct, there must be some contribution from higher-order coupling effects as equation (17) allows only for softening. First-order character for the high-pressure transition in spodumene results in larger discontinuities for the elastic constants at the transition point than would occur at a classical second-order transition. Many of the individual elastic constants of the $P2_1/c$ structure are expected to have a nonlinear dependence on pressure and this gives the bulk modulus a marked curvature. This curvature probably provides a more physically realistic description of the bulk modulus than is obtained simply by fitting a Murnaghan equation of state to the volume data.

[34] Details of the observed elastic constant variations are not quite the same as predicted using a simple Landau expansion. Uncertainties in the pressure calibrations probably account for self-evident problems with data for the first measurement of V_p in the A direction. The general trends of the elastic constant variations were nevertheless duplicated in separate measurements for all three directions. If the pressures are uncertain, then there is an added uncertainty in using compressibility data from *Arlt and Angel* [2000a] to calculate the sample length when converting traveltimes to velocities. Again, however, there is not much ambiguity about where the transition occurs in the uncalibrated traveltimes (Figure 2), at least for A and C directions. Slightly different choices for the sample lengths would not modify the overall pattern of elastic constant variations. Finally, the bare elastic constants are unlikely to be linearly dependent on pressure over the full 10 GPa range, but the introduction

of some curvature is unlikely to account for all the discrepancies. If the experimental data are more or less correct, it necessarily follows that the Landau expansion provides an incomplete description of the transition. The fact that the independently determined strain variations [*Arlt and Angel*, 2000a] are also not consistent with couplings of the form λeQ^2 is consistent with this view. Higher-order strain/order parameter couplings might be implicated, in which case spodumene is only the third silicate mineral, after albite and quartz [*Carpenter et al.*, 1998a, 1998b; *Carpenter and Salje*, 1998] with this unusual characteristic. An independent determination of the evolution of the order parameter would permit a more definitive analysis of the nature of this coupling.

[35] There are small details in the experimental elastic constant variations which also appear to be reproducible. For example, there is a slight softening in the $C2/c$ structure ahead of the transition point for both sets of C_B data and for one set of each of C_A and C_C. Equivalent softening of a coelastic or improper ferroelastic transition as a function of temperature can be understood in terms of fluctuations [*Carpenter and Salje*, 1998, and references therein]. This softening is restricted to elastic constants which have symmetry properties related to those of the identity representation and depends on details of the dispersion of soft branches of the phonon spectrum around the critical point of the soft mode in the Brillouin zone. The effect is well known in quartz [*Carpenter et al.*, 1998b, and references therein], gadolynium molybdate [*Höchli*, 1972], $KMnF_3$ perovskite [*Cao and Barsch*, 1988] and $SrTiO_3$ [*Carpenter and Salje*, 1998] but, as far as the present authors are aware, has not previously been reported for a phase transition driven by pressure.

[36] A second reproducible detail of the elasticity measurements is the marked attenuation which occurs close to the transition point for all runs in which C_A and C_B were measured (Figure 7). This is a characteristic feature of thermodynamically continuous displacive transitions, such as the cubic $\leftrightarrow$ tetragonal transition in $SrTiO_3$ [*Berre et al.*, 1969; *Fossheim and Berre*, 1972; *Fossum and Fossheim*, 1985; *Deorani et al.*, 1990]. For a first-order transition, attenuation due to fluctuations is less likely to occur because the order parameter susceptibility does not tend to zero at the transition point. For spodumene, an alternative cause is, perhaps, the interaction of sound waves with interfaces between $C2/c$ and $P2_1/c$ regions. *Arlt and Angel* [2000b] showed that such interfaces persist over a small pressure interval around P_{tr} and that they are highly mobile. Local stresses close to an interface of this type during the passage of a sound wave could cause it to be displaced, with a loss of energy which would be evident at a macroscopic scale as attenuation. This is analogous to the effect of twin walls in ferroelastic materials [e.g., *Harrison and Redfern*, 2002; *Harrison et al.*, 2003], except that the interfaces only exist in the stability field of coexisting $C2/c$ and $P2_1/c$ structures. The pattern for the C direction is quite different, however. In this orientation, an abrupt increase in attenuation occurs as the transition point is approached from below, but returns gradually to the main trend at $\sim$6.5 GPa (Figure 7). Within a range of $\sim$1 GPa above the transition point, the attenuation is accompanied by rather low (and reproducible) values of C_C. An anelastic origin comparable to the effect of twin walls requires that the two phase field is much wider than for the other two orientations. This seems implausible and the anomalies further emphasize that the mechanism of the $C2/c \leftrightarrow P2_1/c$ transition in spodumene remains only poorly understood. Measurements of the other elastic constants (and attenuation effects) should be revealing of other structural changes which occur but which are not accounted for explicitly in (5).

[37] It has been assumed throughout the present analysis that the pressure seen by each spodumene crystal in the multianvil assembly is close to being hydrostatic. A uniaxial stress regime, with unique axis parallel to the cylinder axis of the crystal and axial stress greater in magnitude than radial stress, would favor the $P2_1/c$ phase if the linear strain accompanying the phase transition in the axial direction of the crystal was negative. It would favor the $C2/c$ structure if the linear strain was positive. On this basis the transition pressure would be expected to be lower for direction C than direction B of the spodumene crystals. Transition pressures deduced from the traveltime data are at least consistent with this suggestion.

[38] Although a complete set of elastic constants has not been determined and the Landau model may be incomplete, there are enough data to show how the phase transition would change the bulk elastic properties of a polycrystalline sample of spodumene. Variations of all the elastic constants, as calculated using (16)–(25) and values of the parameters listed in Table 3, are shown in Figure 10a. Values of λ_4 and λ_6 are not known and have been set arbitrarily to 100 GPa. Some pressure dependence was included for all the bare elastic constants, apart from C^o_{15}, C^o_{25}, C^o_{35} and C^o_{46}. Pressure derivatives were set arbitrarily at 6 for C^o_{11}, C^o_{22}, C^o_{22} and 2 for C^o_{12}, C^o_{13}, C^o_{23}, C^o_{44}, C^o_{55}, C^o_{66}. Voigt, Reuss and Voigt/Reuss average values for the bulk and shear moduli are shown in Figure 10b. A constant density of 3.182 g cm^{-3} was used to calculate compressional and shear wave velocities (V_p, V_s) from these, and the resulting variations are shown in Figure 10c. The transition is characterized by a large volume strain which is then manifest in the large drop in bulk modulus at the transition point. This, in turn, causes the drop in velocity of compressional waves. Shear wave velocities through a polycrystalline sample would be much less affected by the transition if the coupling coefficients λ_4 and λ_6 are only $\sim$100 GPa. A discontinuity in V_s should, nevertheless, be expected (Figure 10c).

[39] Calibration of all the coefficients in (5) permits the free energy change due to the phase transition to be determined. Again using the parameters listed in Table 3, the free energy change due to the phase transition would be -3.5 kJ mole^{-1} at 7 GPa. Of this, terms in Q alone contribute +0.5 kJ mole^{-1}, strain/order parameter coupling terms contribute -8.0 kJ mole^{-1} and the Hooke's law elastic energy contribution is +4.0 kJ mole^{-1}. (A constant molar volume of 5.86×10^{-5} m^3 mole^{-1} was used to convert the energy from units of GPa to J mole^{-1}). Thus the symmetry breaking mechanism for the transition, presumably a soft optic mode, provides only a small proportion of the total driving energy. The energy reduction comes overwhelmingly from strain relaxations which couple with the driving order parameter and substantially stabilize the $P2_1/c$ structure.

[40] Structural phase transitions in quartz and stishovite also cause substantial anomalies in elastic properties. Details of the transition mechanisms differ, however, with

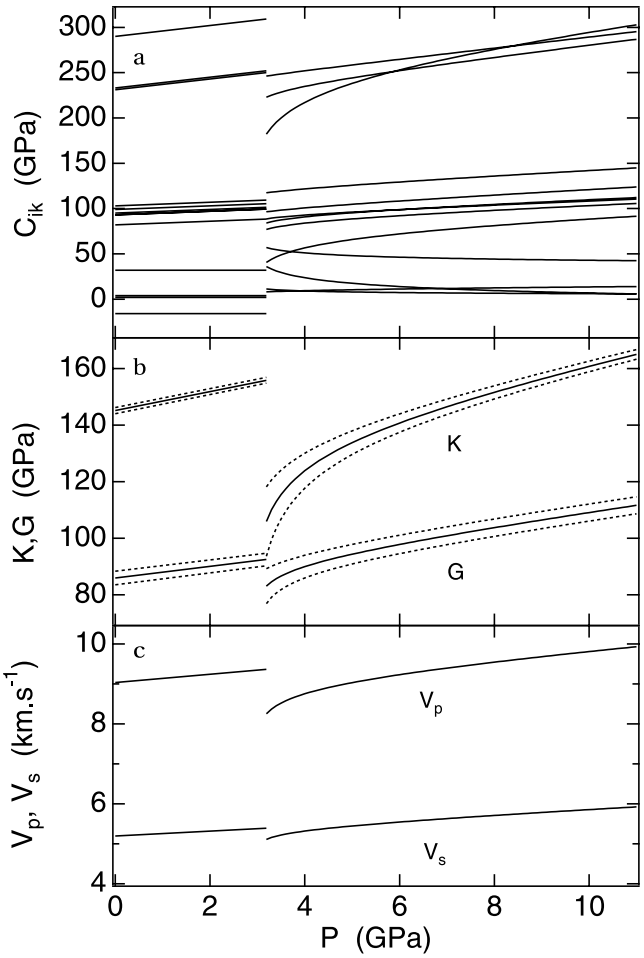

Figure 10. Solutions for the elastic properties of spodumene, as calculated using the parameters listed in Table 3. (a) Individual elastic constants, which can be identified by noting the values of the bare elastic constants given in Table 3. A slope of 6 was assigned to C_{11}^{o}, C_{22}^{o}, and C_{33}^{o}, and a slope of 2 was assigned to C_{12}^{o}, C_{13}^{o}, C_{23}^{o}, C_{44}^{o}, C_{55}^{o}, and C_{66}^{o}. (b) Bulk and shear moduli derived from single-crystal elastic constants shown in Figure 10a. Dotted lines are Voigt and Reuss values. Solid lines are Voigt/Reuss averages. (c) Variations of compressional and shear wave velocities (V_p, V_s) for polycrystalline spodumene, as calculated using the Voigt/Reuss average values of bulk and shear moduli and a constant value for density.

the result that distinctive patterns of elastic behavior for each transition might become indicative evidence of that transition taking place at depth in the Earth. In quartz, the softening is observed effectively only in the bulk modulus [*Kern*, 1979, 1982; *Carpenter et al.*, 1998b; *Carpenter*, 2006]. In stishovite, the high-pressure transition is expected to be accompanied by a large softening of the bulk and shear moduli over a wide interval as the transition point is approached from the high-symmetry side as well as from the low-symmetry side [*Karki et al.*, 1997; *Carpenter et al.*, 2000; *Hemley et al.*, 2000]. These transitions in SiO_2 phases have recently been identified as possible causes of seismic anomalies. *Mechie et al.* [2004] and *Marini and Manzella* [2005] observed reflecting layers in silica rich crust at appropriate conditions for the $\alpha \leftrightarrow \beta$ quartz transition. *Hirose et al.* [2005] have discussed seismic features at depths of ~1400–1600 km in subducted MORB crust in terms of the tetragonal $\leftrightarrow$ orthorhombic transition in stishovite. Geophysical markers of this type are potentially invaluable for providing information on temperature and composition at depth, first, because they can be significantly sharper than the anomalies which are due to reconstructive transitions and, secondly, because they have *PT* trajectories which can be tightly constrained using experimental or computational methods. An advantage of Landau-type descriptions in this context is that they provide a robust method of analyzing or extrapolating elastic behavior as a function of both temperature and pressure.

[41] Whether or not there are further structural phase transitions to be discovered in deep crustal, mantle or core minerals is a matter for future research, but improving geophysical methods are leading to the discovery of new seismic anomalies with finer and finer resolution [e.g., *Deuss and Woodhouse*, 2001, 2002]. These will no doubt be interpreted in the usual way by comparing observed patterns of elasticity with patterns expected from different mechanisms: reconstructive transitions, displacive transitions, preferred crystallographic orientations, etc. Understanding the distinctive form of the anomalies due to structural phase transitions from strain and elasticity measurements of the type presented in this paper will clearly be relevant to this process. From the insights gained from the present study of spodumene, it is clear that a $C2/c \leftrightarrow P2_1/c$ transition in crustal or mantle pyroxene could give rise to a reflecting plane for seismic waves. The same symmetry change occurs in monoclinic end-member $MgSiO_3$ at ~6–7 GPa and ~0–800°C [*Gasparik*, 1990; *Angel et al.*, 1992; *Angel and Hugh-Jones*, 1994; *Kung et al.*, 2004], for example, though in this case the high-pressure form has $C2/c$ symmetry and the low-pressure form has $P2_1/c$ symmetry. Even if the actual transition point is not reached, the influence of a transition mechanism on elastic softening might still be important. In the case of orthorhombic $MgSiO_3$, an analogous transition with a symmetry change of *Cmca* $\leftrightarrow$ *Pbca* has been proposed by *Jackson et al.* [2004]. This is believed to be responsible for substantial nonlinear softening of single-crystal elastic constants at high temperatures. The displacive transition itself is not observed because an alternative reconstructive transition occurs and it is even possible that the elastic softening of the former acts as a trigger for the latter. Similarly, *Kung et al.* [2004] observed nonlinear changes in the bulk and shear moduli of orthoenstatite ahead of a reconstructive transition to clinoenstatite at high pressures. The essential issues in all these examples relate to the fundamental fact that structural phase transitions are frequently associated with or driven by substantial changes in elastic properties.

[42] **Acknowledgments.** This work was supported by grant NER/A/S/2000/01055 from the Natural Environment Research Council of Great Britain, which is gratefully acknowledged. The ultrasonic experiments were performed in the Stony Brook High Pressure Laboratory, with partial support of NSF grants to B.L. (EAR0003340) and to R.C.L. (EAR02-29704). The authors also thank Ross Angel for his help in providing data for spodumene obtained at high pressures in the diamond anvil cell.

References

Agee, C. B. (1998), Phase transformations and seismic structure in the upper mantle and transition zone, in *Ultrahigh-Pressure Mineralogy*,

Rev. Mineral., vol. 37, edited by R. J. Hemley, pp. 165–203, Mineral. Soc. of Am., Washington, D. C.

Aleksandrov, K. A., and G. T. Prodaivoda (1993), Elastic properties of minerals, *Crystallogr. Rep.*, *38*, 698–709.

Angel, R. J., and D. A. Hugh-Jones (1994), Equations of state and thermodynamic properties of enstatite pyroxenes, *J. Geophys. Res.*, *99*, 19,777–19,783.

Angel, R. J., A. Chopelas, and N. L. Ross (1992), Stability of high-density clinoenstatite at upper-mantle pressures, *Nature*, *358*, 322–324.

Arlt, T., and R. J. Angel (2000a), Displacive phase transitions in C-centred clinopyroxenes: Spodumene, $LiScSi_2O_6$ and $ZnSiO_3$, *Phys. Chem. Miner.*, *27*, 719–731.

Arlt, T., and R. J. Angel (2000b), Pressure buffering in a diamond anvil cell, *Min. Mag.*, *64*, 241–245.

Arlt, T., R. J. Angel, R. Miletich, T. Armbruster, and T. Peters (1998), High-pressure P21/c-C2/c phase transitions in clinopyroxenes: Influence of cation size and electronic structure, *Am. Mineral.*, *83*, 1176–1181.

Arlt, T., M. Kunz, J. Stolz, T. Armbruster, and R. J. Angel (2000), P-T-X data on P21/c-clinopyroxenes and their displacive phase transitions, *Contrib. Mineral. Petrol.*, *138*, 35–45.

Berre, B., K. Fossheim, and K. A. Müller (1969), Critical attenuation of sound by soft modes in $SrTiO_3$, *Phys. Rev. Lett.*, *23*, 589–591.

Cao, W., and G. R. Barsch (1988), Elastic constants of $KMnF_3$ as functions of temperature and pressure, *Phys. Rev. B*, *38*, 7947–7958.

Carpenter, M. A. (2006), Elastic properties of minerals and the influence of phase transitions, *Am. Mineral.*, *91*, 229–246.

Carpenter, M. A., and E. K. H. Salje (1998), Elastic anomalies in minerals due to structural phase transitions, *Eur. J. Mineral.*, *10*, 693–812.

Carpenter, M. A., E. K. H. Salje, and A. Graeme-Barber (1998a), Spontaneous strain as a determinant of thermodynamic properties for phase transitions in minerals, *Eur. J. Mineral.*, *10*, 621–691.

Carpenter, M. A., E. K. H. Salje, A. Graeme-Barber, B. Wruck, M. T. Dove, and K. S. Knight (1998b), Calibration of excess thermodynamic properties and elastic constant variations associated with the $\alpha \leftrightarrow \beta$ phase transition in quartz, *Am. Mineral.*, *83*, 2–22.

Carpenter, M. A., R. J. Hemley, and H. K. Mao (2000), High-pressure elasticity of stishovite and the P42/mnm $\leftrightarrow$ Pnnm phase transition, *J. Geophys. Res.*, *105*, 10,807–10,816.

Darling, K. L., G. D. Gwanmesia, J. F. Kung, B. Li, and R. C. Liebermann (2004), Ultrasonic measurements of the sound velocities in polycrystalline San Carlos olivine in multi-anvil, high-pressure apparatus, *Phys. Earth Planet. Inter.*, *143–144*, 19–31.

Decremps, F., J. Zhang, B. Li, and R. C. Liebermann (2001), Pressure-induced softening of shear modes in ZnO, *Phys. Rev. B*, *63*, 224105.

Deorani, S. C., U. C. Naithani, and B. S. Semwal (1990), Ultrasonic attenuation in $SrTiO_3$ perovskite above the phase transition, *J. Phys. Chem. Solids*, *51*, 1277–1280.

Deuss, A., and J. H. Woodhouse (2001), Seismic observations of splitting of the mid-transition zone discontinuity in Earth's mantle, *Science*, *294*, 345–357.

Deuss, A., and J. H. Woodhouse (2002), A systematic search for mantle discontinuities using SS-precursors, *Geophys. Res. Lett.*, *29*(8), 1249, doi:10.1029/2002GL014768.

Fossheim, K., and B. Berre (1972), Ultrasonic propagation, stress effects, and interaction parameters at the displacive transition in $SrTiO_3$, *Phys. Rev. B*, *5*, 3292–3308.

Fossum, J. O., and K. Fossheim (1985), Measurements of ultrasonic attenuation and velocity in Verneuil-grown and flux-grown $SrTiO_3$, *J. Phys. C*, *18*, 5549–5578.

Gasparik, T. (1990), A thermodynamic model for the enstatite-diopside join, *Am. Mineral.*, *75*, 1080–1091.

Harrison, R. J., and S. A. T. Redfern (2002), The influence of transformation twins on the seismic-frequency elastic and anelastic properties of perovskite: Dynamical mechanical analysis of single crystal $LaAlO_3$, *Phys. Earth Planet. Inter.*, *134*, 253–272.

Harrison, R. J., S. A. T. Redfern, and J. Street (2003), The effect of transformation twins on the seismic-frequency mechanical properties of polycrystalline $Ca_{1-x}Sr_xTiO_3$ perovskite, *Am. Mineral.*, *88*, 574–582.

Haussühl, S. (1993), Interpretation of elastic properties of ionic crystals: Validity of a quasi-additivity rule?, *Z. Kristallogr.*, *205*, 215–234.

Hemley, R. J., J. F. Shu, M. A. Carpenter, J. Hu, H.-K. Mao, and K. J. Kingma (2000), Strain/order parameter coupling in the ferroelastic transition in dense SiO_2, *Solid State Commun.*, *114*, 527–532.

Hirose, K., N. Takafuji, N. Sata, and Y. Ohishi (2005), Phase transition and density of subducted MORB crust in the lower mantle, *Earth Planet. Sci. Lett.*, *237*, 239–251.

Höchli, U. T. (1972), Elastic constants and soft optical modes in gadolinium molybdate, *Phys. Rev. B*, *6*, 1814–1823.

Jackson, J. M., S. V. Sinogeikin, M. A. Carpenter, and J. D. Bass (2004), Novel phase transition in orthoenstatite, *Am. Mineral.*, *89*, 239–245.

Karki, B. B., L. Stixrude, and J. Crain (1997), Ab initio elasticity of three high-pressure polymorphs of silica, *Geophys. Res. Lett.*, *24*, 3269–3272.

Kern, H. (1979), Effect of high-low quartz transition on compressional and shear wave velocities in rocks under high pressure, *Phys. Chem. Miner.*, *4*, 161–171.

Kern, H. (1982), Elastic-wave velocity in crustal and mantle rocks at high pressure and temperature: The role of the high-low quartz transition and of dehydration reactions, *Phys. Earth Planet. Inter.*, *29*, 12–23.

Kung, J., B. Li, T. Uchida, Y. Wang, D. Neuville, and R. C. Liebermann (2004), In situ measurements of sound velocities and densities across the orthopyroxene $\rightarrow$ high-pressure clinopyroxene transition in $MgSiO_3$ at high pressure, *Phys. Earth Planet. Inter.*, *147*, 27–44.

Levien, L., D. J. Weidner, and C. T. Prewitt (1979), Elasticity of diopside, *Phys. Chem. Miner.*, *4*, 105–113.

Li, B., I. Jackson, T. Gasparik, and R. C. Liebermann (1996), Elastic wave velocity measurement in multi-anvil apparatus to 10 GPa using ultrasonic interferometry, *Phys. Earth Planet. Inter.*, *98*, 79–91.

Li, B., K. Chen, J. Kung, R. C. Liebermann, and D. J. Weidner (2002), Sound velocity measurement using transfer function method, *J. Phys. Condens. Matter*, *14*, 11,337–11,342.

Liebermann, R. C., and B. Li (1998), Elasticity at high pressures and temperatures, in *Ultrahigh-Pressure Mineralogy*, *Rev. Mineral.*, vol. 37, edited by R. J. Hemley, pp. 459–492, Mineral. Soc. of Am., Washington, D. C.

Marini, L., and A. Manzella (2005), Possible seismic signature of the α-β quartz transition in the lithosphere of southern Tuscany (Italy), *J. Volcanol. Geotherm. Res.*, *148*, 81–97.

Mechie, J., S. V. Sobolev, L. Ratschbacher, A. Y. Babeyko, G. Bock, A. G. Jones, K. D. Nelson, K. D. Solon, L. D. Brown, and W. Zhao (2004), Precise temperature estimation in the Tibetan crust from seismic detection of the α-β quartz transition, *Geology*, *32*, 601–604.

Migliori, A., T. W. Darling, J. P. Baiardo, and F. Freibert (2001), Resonant ultrasound spectroscopy (RUS), in *Dynamic Methods for Measuring the Elastic Properties of Solids: Handbook of Elastic Properties of Solids, Liquids, and Gases*, vol. I, edited by A. G. Every and W. Sachse, pp. 239–262, Elsevier, New York.

Nelson, D. F. (Ed.) (1992), *Landolt-Bornstein: Group III: Crystal and Solid State Physics: Low Frequency Properties of Dielectric Crystals: Subvolume A: Second and Higher Order Elastic Constants*, Springer, New York.

Niesler, H., and I. Jackson (1989), Pressure derivatives of elastic wave velocities from ultrasonic interferometric measurements on jacketed polycrystals, *J. Acoust. Soc. Am.*, *86*, 1573–1585.

Pommier, C. J. S., M. B. Denton, and R. T. Downs (2003), Raman spectroscopic study of spodumene ($LiAlSi_2O_6$) through the pressure-induced phase change from C2/*c* to $P2_1/c$, *J. Raman Spectrosc.*, *34*, 769–775.

Redfern, S. A. T., and E. K. H. Salje (1987), Thermodynamics of plagioclase II: Temperature evolution of the spontaneous strain at the $I1 \leftrightarrow P1$ phase-transition in anorthite, *Phys. Chem. Miner.*, *14*, 189–195.

Schlenker, J. L., G. V. Gibbs, and M. B. Boisen Jr. (1978), Strain-tensor components expressed in terms of lattice parameters, *Acta Crystallogr., Sect. A*, *34*, 52–54.

Schreuer, J. (2002), Elastic and piezoelectric properties of $La_3Ga_5SiO_{14}$ and $La_3Ga_{5.5}Ta_{0.5}O_{14}$: An application of resonant ultrasound spectroscopy, *IEEE Trans. Ultrason. Ferroelectr. Frequency Control*, *49*, 1474–1479.

Slonczewski, J. C., and H. Thomas (1970), Interaction of elastic strain with the structural transition of strontium titanate, *Phys. Rev. B*, *1*, 3599–3608.

M. A. Carpenter and P. Sondergeld, Department of Earth Sciences, University of Cambridge, Downing Street, Cambridge CB2 3EQ, UK. (mc43@esc.cam.ac.uk)

B. Li, Department of Geosciences, State University of New York at Stony Brook, Stony Brook, NY 11794, USA.

J. Schreuer, Institut für Mineralogie/Kristallographie, Universität Frankfurt, Senckenberganlage 30, D-60054 Frankfurt am Main, Germany.